NeuroImage 198 (2019) 242–254

Contents lists available at ScienceDirect

NeuroImage

journal homepage: www.elsevier.com/locate/neuroimage

Bidirectional signal exchanges and their mechanisms during joint attention interaction – A hyperscanning fMRI study

Gadi Goelman [a,*,1], Rotem Dan [a,b], Gabriela Stößel [c,2], Heike Tost [d,2], Andreas Meyer-Lindenberg [d,2], Edda Bilek [d,2]

[a] Department of Neurology, Hadassah Medical Center, The Hebrew University Medical School, Jerusalem, Israel
[b] Edmond and Lily Safra Center for Brain Sciences, The Hebrew University of Jerusalem, Jerusalem, Israel
[c] Department of Clinical Psychology, Germany
[d] Department of Psychiatry and Psychotherapy, Central Institute of Mental Health, Medical Faculty Mannheim, University of Heidelberg, Mannheim, Germany

ARTICLE INFO

Keywords:
Joint attention
Hyperscanning
Multivariate analysis
Directed functional connectivity
Bidirectional flow

ABSTRACT

Social interactions are essential to our daily life. We tested the hypothesis that social interactions during joint attention (JA) require bidirectional communication, each with a different mechanism. We used a novel multivariate functional connectivity analysis, which enables obtaining directed pathways between four regions at each time-frequency point, with hyper-scanning MRI data of real-time JA interaction. Constructing multiple "4-regional directed pathways" and counting the number of times, regions engaged in feedforward or feedback processes in the 'sender' or the 'receiver brains, we obtained the following. (1) There were more regions in feedforward than in feedback processes (125 versus 99). (2) The right hemisphere was more involved in feedforward (74 versus 33), while the left hemisphere in feedback (66 versus 51). (3) The dmPFC was more engaged in feedforward (73 versus 44) while the TPJ in both (49 versus 45). (4) The dmPFC was more involved in the sending processes (i.e. initiation of feedforward and feedback) while the TPJ in the receiving processes. (5) JA interaction was involved with high MRI frequencies (0.04–0.1 Hz), while continues interactions by low MRI frequencies (0.01–0.04 Hz). (6) Initiation and responding to JA (i.e. IJA and RJA) evolved with composite neural systems: similar systems for pathways that included the dmPFC, vmPFC and the STS, and different systems for pathways that included the TPJ, vmPFC, PCC and the STS. These findings have important consequences in the basic understanding of social interaction and could help in diagnose and follow-up of social impairments.

1. Introduction

The ability to communicate, verbally and nonverbally, is a basic human skill and need, which affects individuals as well as society development and organization. It encompasses social interaction, social cognition, pragmatics, and language processing. Natural social contact is usually reciprocal, i.e., when connecting with others, one will most likely receive a response (although possibly non-verbal) to own actions and statements which shapes the immediate cognitive and emotional state of the individual (Hari et al., 2015) (Schilbach et al., 2013). Research in this highly unpredictable context requires a balance between ecological validity and methodological advancement(Schilbach et al., 2013). This has been pioneered by hyper-scanning protocols, where magnetic resonance imaging (MRI), electroencephalography, or near-infrared spectroscopy set-ups were constructed to enable simultaneous data acquisition in interacting individuals(Babiloni and Astolfi, 2014).

Previous hyper-scanning studies have shown that brain systems of subjects synchronize during interactions, that this synchronization is specific to true social contacts and takes place only during the interaction (Bilek et al., 2015; Koike et al., 2016; Balconi and Vanutelli, 2017; Bilek et al., 2017; Liu et al., 2018). Such synchronization resembles the flow of information between brain systems of interacting human subject pairs (Schippers et al., 2010). Moreover, this synchronization was distorted in subject pairs that involved a patient with Borderline Personality disorder, a disorder that encompasses severe difficulties in the building and maintenance of relationships as well as daily interactions (Bilek et al., 2017). The discovery of a disrupted two-brain marker in a mental disorder highlights the clinical relevance of hyper-scanning studies: many

* Corresponding author. Department of Neurology, Hadassah Hebrew University Medical Center, Jerusalem, 91120, Israel.
E-mail address: gadig@hadassah.org.il (G. Goelman).
[1] The author takes responsibility for the integrity of the data analysis and conclusions.
[2] Authors take responsibility for the experimental paradigm, data acquisition, and fMRI data.

https://doi.org/10.1016/j.neuroimage.2019.05.028
Received 29 January 2019; Received in revised form 1 May 2019; Accepted 10 May 2019
Available online 18 May 2019
1053-8119/

psychiatric conditions are diagnosed based on observable social behavior, while the neural underpinnings are mostly unknown because of exclusive use of non-interactive studies examining only one person (Schilbach et al., 2013). A disruption of the ability to synchronize brain activity with a partner may be useful in the tailoring of individualized psychiatric care and/or predict therapy outcome. Our previous approach underscores the relevance of the synchronization of neural systems but was not able to estimate directionality of the information flow. However, the core definition of "real" social contact as involving reciprocity assumes a flow of information in both directions between subjects, possibly involving specific temporal hierarchies across different frequency bands.

Recently we introduced a novel directed functional connectivity method that is based on nonlinear coherences in frequency-time space and demonstrated its use with resting state fMRI data (Goelman and Dan, 2017a). We have shown that for groups of four coupled BOLD signals, each from a different anatomical location, the rank (or the hierarchy) of the temporal order of these signals can be obtained analytically by nonlinear coherences at each time-frequency point. Phase differences at a given frequency resembled the time differences (i.e., time lag) and therefore define temporal order. Notably, obtaining the mutual coherence of four signals simultaneously states a clear novelty for a temporal coherence approach, rather than pairwise coherences (Goelman and Dan, 2017a; Goelman et al., 2018). Our new method considers higher order mutual information (characterized by phases of complex wavelet coefficients) which constitutes a multivariate measure versus the bivariate measure used in pairwise coherence. Mutual interaction can be concluded when the four regions are coupled and are part of a common process that includes information transfer among the four regions. There are four novel aspects in the new analysis: (1) defining "4-regional networks" of mutual interaction; (2) finding the temporal hierarchy among the region's time-series; (3) defining directionality in which the interaction occurs and (4) referring a frequency to the interaction.

For the present study, we modified and extended our multivariate analysis to enable obtaining dynamic information and thus to define directed pathways of information transfer between two individuals during joint attention (JA) interaction at each time-frequency point. We hypothesize that inter-individual communication, even for the simple JA paradigm includes some form of information exchange between the individuals. Our analysis enables testing the following critical questions: (1) Are responding JA (RJA) and initiating JA (IJA) processes having an equal neural system? (2) Is JA including a feedback response? (3) In the case of feedback, are initiation and receiving feedback processes having equal neural systems? (4) Are JA processes in the right and the left hemispheres similar? Moreover, (5) are these processes frequency dependent. Here we test these questions by using real-time communication measurements during JA interaction together with our novel analysis method. For this purpose, we used previously acquired hyperscanning JA data (Bilek et al., 2015).

2. Methods

2.1. Theory - directed multivariate analysis among 4 time-series

Recently we have shown that the mutual interaction between 4 coupled time-series (specifically, the BOLD contrast fMRI signals of 4 different brain regions) can be expressed by their nonlinear mutual coherences at each time-frequency point (Goelman and Dan, 2017a). It included a full mathematical derivation and a strategy to extend it to high number of time-series. This extension was not done yet therefore, the current analysis is limited to four time-series i.e. four regions. To validate the mathematical derivations along with the effects of coupling strength and noise, computer simulations using the Kuramoto coupled oscillator model was used. Simulations demonstrated correct directionality for a large range of coupling strength and low sensitivity to Gaussian noise compared with pairwise coherences (Goelman and Dan, 2017a).

The three mutual coherences (termed in hereafter "functional connectivity", FC) equal:

$$\begin{aligned} FC^{1}_{j1,j2,j3,j4}(\omega,t) &= \left(W^{j1}_{\omega,t}\right)\cdot\left(W^{j2}_{\omega,t}\right)^{*}\cdot\left(W^{j3}_{\omega,t}\right)\cdot\left(W^{j4}_{\omega,t}\right)^{*} = A\cdot\left\{\exp\left[i\left(\vartheta^{j1}_{\omega,t}-\vartheta^{j2}_{\omega,t}+\vartheta^{j3}_{\omega,t}-\vartheta^{j4}_{\omega,t}\right)\right]\right\} = Ae^{i\varphi^{a}} \\ FC^{2}_{j1,j2,j3,j4}(\omega,t) &= \left(W^{j1}_{\omega,t}\right)\cdot\left(W^{j2}_{\omega,t}\right)\cdot\left(W^{j3}_{\omega,t}\right)^{*}\cdot\left(W^{j4}_{\omega,t}\right)^{*} = A\cdot\left\{\exp\left[i\left(\vartheta^{j1}_{\omega,t}+\vartheta^{j2}_{\omega,t}-\vartheta^{j3}_{\omega,t}-\vartheta^{j4}_{\omega,t}\right)\right]\right\} = Ae^{i\varphi^{b}} \\ FC^{3}_{j1,j2,j3,j4}(\omega,t) &= \left(W^{j1}_{\omega,t}\right)\cdot\left(W^{j2}_{\omega,t}\right)^{*}\cdot\left(W^{j3}_{\omega,t}\right)^{*}\cdot\left(W^{j4}_{\omega,t}\right) = A\cdot\left\{\exp\left[i\left(\vartheta^{j1}_{\omega,t}-\vartheta^{j2}_{\omega,t}-\vartheta^{j3}_{\omega,t}+\vartheta^{j4}_{\omega,t}\right)\right]\right\} = Ae^{i\varphi^{c}} \end{aligned} \quad (1)$$

where, $W^{j1}_{\omega,t}$ is the wavelet coefficient in time and frequency of time-series '*j1*', $\vartheta^{j1}_{\omega,t}$ is the phase of time-series '*j1*', '*A*' is the coherence amplitude, * denotes the complex conjugate and '*i*' is the imaginary unit. The nonlinear coherence phases, φ^{a}, φ^{b}, and φ^{c}, are computed according to Equation (1) and were used to obtain the phases of the time-series for each frequency and time point (Goelman and Dan, 2017a):

$$\begin{aligned} \vartheta^{j2}_{\omega,t} &= \vartheta^{j1}_{\omega,t}\mp\frac{\varphi^{a}+\varphi^{c}}{2};\quad \vartheta^{j3}_{\omega,t} = \vartheta^{j1}_{\omega,t}\mp\frac{\varphi^{b}+\varphi^{c}}{2};\quad \vartheta^{j4}_{\omega,t} = \vartheta^{j1}_{\omega,t}\mp\frac{\varphi^{a}+\varphi^{b}}{2} \\ \vartheta^{j2}_{\omega,t} &= \vartheta^{j3}_{\omega,t}\mp\frac{\varphi^{a}-\varphi^{b}}{2};\quad \vartheta^{j4}_{\omega,t} = \vartheta^{j3}_{\omega,t}\mp\frac{\varphi^{a}-\varphi^{c}}{2};\quad \vartheta^{j4}_{\omega,t} = \vartheta^{j2}_{\omega,t}\mp\frac{\varphi^{b}-\varphi^{c}}{2} \end{aligned} \quad (2)$$

where $\mp$ is due to the freedom in the phase definition which requires specification of the sign (Goelman and Dan, 2017a). To obtain pathways between 4 coupled time-series, i.e. their temporal hierarchy which

Table 1
A list of continues pathways in the 4-regional networks. R1 to R4 are the four regions (i.e., network nodes) from which time-series are taken.

PW number	Pathway
1	R1-R2-R3-R4
2	R2-R3-R4-R1
3	R3-R4-R1-R2
4	R4-R1-R2-R3
5	R1-R2-R4-R3
6	R2-R4-R3-R1
7	R3-R1-R2-R4
8	R4-R3-R1-R2
9	R1-R3-R4-R2
10	R3-R4-R2-R1
11	R4-R2-R1-R3
12	R2-R1-R3-R4
13	R1-R4-R3-R2
14	R2-R1-R4-R3
15	R3-R2-R1-R4
16	R4-R3-R2-R1
17	R1-R3-R2-R4
18	R2-R4-R1-R3
19	R3-R2-R4-R1
20	R4-R1-R3-R2
21	R1-R4-R2-R3
22	R2-R3-R1-R4
23	R3-R1-R4-R2
24	R4-R2-R3-R1

describes how information is transferred among them, we assume that phases (i.e. coherences or phase-differences) at specific frequencies contain temporal information (i.e. time-lags). Furthermore, we assume that all regions have comparable hemodynamic responses (Goelman et al., 2018). If we restrict the analysis to continuous paths, i.e., a pathway that starts at one region and subsequently goes through all other regions, then a network of 4 time-series has 24 possible continuous paths (Goelman et al., 2018). Table 1 lists all possible continuous pathways in a 4-regional network. Using phase-differences to define temporal hierarchy requires choosing a reference phase. Note that in Equation (2) the phase was of the first time-series ($\vartheta^{j1}_{\omega,t}$). In principle, pathways are independent on this choice unless some phase-differences exceeds 2π.To obtain pathways that are independent on the reference choice and on the 2π limitation, we performed the pathway calculations four times, each with a different reference phase, and only pathways that were invariant to the reference phase were excepted.

We first define a pathway index (PWI). For this we adopted the common approach used in coherence studies, i.e. we calculated (for each time-frequency point and each reference phase) a pathway index as follows (Goelman et al., 2018):

$$PWI^{k}_{ref}(\omega,t)=\frac{1}{N}\sum_{i=1}^{N}\left\{\begin{matrix}1\\0\end{matrix}\right\}\begin{matrix}phases\ in\ line\ with\ the\ pathway\\phases\ not\ in\ line\ with\ the\ pathway\end{matrix} \quad (3)$$

where 'k' is a specific pathway (k = 1,2,…24), 'ref' (1..4) is one of the 4 phase references and *N* is the number of subjects in the group. In Equation (3), we tested for each subject whether the 4 phase-differences of Equation (2) were in line with the '*k*' pathway as given in Table 1. For example, if the relations between the three phase-differences were: $(\vartheta_2-\vartheta_1)<(\vartheta_3-\vartheta_1)<(\vartheta_4-\vartheta_1)$, it suggested that the temporal order between these regions was of pathway # 1 in Table 1 (i.e., 'R1-R2-R3-R4') and $PWI^{pw=1}_{ref=1}(\omega,t)$equals 1 for this subject. Namely, for each subject and each pathway, a value of 1 is assigned when the network phase-differences are in agreement with this pathway, and zero is assigned when there isn't an agreement. Equation (3) is similar to the Phase Lag Index (PLI) (Stam et al., 2007; Stam and van Straaten, 2012). In order to select only pathways that were invariant to the choice of the reference phase and to the 2π limitation, we define the following pathway index that is reference independent:

$$PWI^{k}(\omega,t)=\left\{\begin{matrix}1\\0\end{matrix}\right\}\begin{matrix}PWI^{k}_{1}(\omega,t),>cut\ \textbf{AND}\ PWI^{k}_{2}(\omega,t)>cut\ \textbf{AND}\ PWI^{k}_{3}(\omega,t)>cut\ \textbf{AND}\ PWI^{k}_{4}(\omega,t)>cut\\condition\ not\ met\end{matrix} \quad (4)$$

Permutation-based non-parametric tests with uncoupled time-series were used to obtain the null distributions of Equation (4) for each pathway and each time-frequency point enabling assign a *p*-value for the *cut* value.

2.2. Subjects

64 female subjects were recruited from the population of Mannheim, Germany, and provided written informed consent to participate in the study. The study was approved by the Ethics Committee of Heidelberg University. As described previously (Bilek et al., 2015), subjects were investigated as pairs to undergo fMRI-hyper-scanning. For this, subjects were randomly assigned to a study partner. Data from five pairs were excluded from further analysis because of excessive head movement (3 mm translation or 3° rotation). Concluding, data from 27 pairs (i.e., 54 subjects) with mean age 24.11 ± 4.04 years, mean pair age 48.22 ± 5.46 years, mean with-in pair age difference 4.22 ± 4.27 years; furthermore, mean education 12.69 ±.89 years, mean pair education 25.37 ± 1.21 years, mean with-in pair education difference 0.70 ± 1.10 years underwent data analysis as described below.

2.3. Joint attention paradigm

A detailed description of the JA task used in this study is given elsewhere (Bilek et al., 2015). Briefly, subjects engaged in interaction via eye gaze. In each trial, the information of a target location out of four possible locations was given to one subject (the sender) via on-screen presentation. The sender was asked to pass this information to the other subject (the receiver) via eye movement towards the correct location. This resembles joint attention, a basic form of cooperation as used daily by humans. Each trial was followed by feedback on trial performance. Importantly, subjects saw each other face during the whole experiment. The task included two blocks, each consisting of twenty trials of 10 TRs. In block 'A' one subject was the sender and in block 'B' the other subject was the sender. Order of sender/receiver was randomly assigned and balanced between scanners. Task duration (including trial onset jitter, buffering for scanner synchronization) was 645s. The full task included two scan experiments each of 40 trials (block A and block B).

2.4. MRI-hyperscanning data acquisition

The hyper-scanning set up encompasses two identical scan sites at CIMH, connected via fiber optics transmitting MRI triggers, behavioral data, and live video stream. Each scan site included one Siemens Trio 3T MRI scanner (Siemens, Erlangen, Germany) equipped with custom designed mirror box (MRC Systems GmbH, Heidelberg, Germany) holding the face camera. FMRI data were acquired with the following specifications: TR = 1550 ms, TE = 30 ms, FOV = 192mm2, 64 × 64 slice resolution, 28 slices, 4 mm thickness, 1 mm gap, flip angle 73°, 423/420 vol (triggering/triggered scanner). The same echo-planar imaging protocols were used for both scanners.

2.5. Functional MRI preprocessing and functional connectivity analysis

Standard initial preprocessing was done using Statistical Parametric Mapping (SPM8, Wellcome Trust Center for Neuroimaging, London, United Kingdom, http://www.fil.ion.ucl.ac.uk/spm/software/spm8). Functional images were spatially realigned using a least squares approach and a six parameter (rigid body) spatial transformation. Subsequently, functional images were coregistered to high resolution T1 anatomical images, normalized to Montreal Neurological Institute (MNI) space and resampled at an isotropic voxel size of 2 mm. The normalized images were smoothed with an isotropic 8 mm full-width-at-half-maximum Gaussian kernel. Further preprocessing was done using CONN toolbox (Whitfield-Gabrieli and Nieto-Castanon, 2012) as data was preprocessed for functional connectivity analysis and the effect of stimulus regressed out (see below). Censoring was done according to the method of Power et al. (Power et al., 2014). Confounds were removed by regression, including the six motion parameters, their first order derivatives, scrubbing parameters and 3 principle components of the CSF and the white matter. Prior to the regression of principal components, the white matter and CSF masks were eroded to ensure that only pure white matter or CSF signal was regressed from the data. Potential effects of scan

initiation were removed by applying a step function convolved with the hemodynamic response function. Regression-out of confounds was done to minimize effects of motion and potential physiological and non-neuronal signals such as cardiac and respiratory signals, without the risk of artificially introducing anti-correlations into the functional connectivity estimates (Fox et al., 2009; Murphy et al., 2009; Weissenbacher et al., 2009; Bianciardi et al., 2011; Chai et al., 2011). Last, linear detrending and band-pass filtering (0.008–0.1 Hz) were applied. For quality assurance, the mean framewise displacement (FD), root mean squared movement (RMS) and maximal displacement were calculated based on the six motion parameters derived from the realignment procedure(Power et al., 2014). Rotational displacements were converted from degrees to millimeters by calculating displacement on the surface of a sphere of radius 50 mm, which is approximately the mean distance from the cerebral cortex to the center of the head. The mean framewise displacement was 0.107 ± 0.036, the root mean squared movement 0.487 ± 0.275, and the maximal displacement 0.725 ± 0.497. To test if head motions affected connectivity measures, the FD was correlated with connectivity across subjects. For hypers-canning data and since connectivity was measured between brains, correlations were performed between the sums and the differences of each dyad's FDs on one hand, and the connectivity between brains on the other. Pearson correlations of all time points were close to zero (see results).

2.6. Dynamic directed functional connectivity analysis

All further calculations were performed with IDL version 8.2.0 (Exelis Visual Information Solutions, Inc.) using custom-developed software. Time-frequency pathways were obtained for preselected "4-regional networks". We selected seven **cortical** regions that were shown previously to be involved in social interaction (Van Overwalle, 2009; Schurz et al., 2014; Molenberghs et al., 2016), and constructed "4-regional networks" among them. These regions were: (1) The dorsal medial prefrontal cortex (dmPFC), (2) the temporoparietal junction (TPJ) (masks for these two regions were generously provided by Bzdok(Bzdok et al., 2013)), (3) the ventral medial prefrontal cortex (vmPFC, using the 'frontal_med_orb' AAL mask), (4) the posterior cingulate cortex (PCC, using the 'cingulate_post' AAL mask), (5) the superior temporal sulcus (STS, using the 'temporal_sup' AAL mask), (6) the fusiform gyrus (FFA, using the 'fusiform' AAL mask); (7) and the precuneus (PreCue, using the 'precuneus' AAL mask). We note that more or different regions could be used and we are not claiming that these regions are the only regions that are involved in JA. Only cortical regions were selected since the analysis assumes comparable hemodynamic responses for all regions, and our previous study suggests that non-cortical regions (specifically the basal-ganglia) might have different responses due to their different neurovascular coupling (Goelman et al., 2014). As a result, the reward system and the reward related neuro-circuitry could not be included in full. We note however that the vmPFC includes the orbital frontal cortex which is part of the reward system. Average BOLD signals from these regions, in the left and the right hemispheres, were extracted from each subject and the effect of the stimulus was removed by regression using the eventrelated convolution of the stimulus with the canonical HRF. Temporal BOLD signals were Wavelet transformed using the complex Morlet wavelet functions. We used 4.5 for the smallest scale, 1.55 for the time resolution and 25 scales to cover the entire frequency window. Wavelet software was provided by C. Torrence and G. Compo available at: http://paos.colorado.edu/research/wavelets (Torrence and Compo, 1998).

2.7. Obtaining 'sender' and 'receiver' time-frequency points

Equation (1) was used to calculate the three mutual coherences for each "4-regional network" resulting in three complex time-frequency functions of 416 time-points and 25 frequency points. Next, we averaged (in the time-frequency space) along the 20 trials of block A (where one is the sender) and of block B (when the second is the sender). For this, we used the corresponding TRs of experiment 1 and experiment 2 to obtain the time-frequency points of the brain when it was 'sending' information, and the time-frequency points of the brain when it was 'receiving' information. These resulted with six complex expressions, each of 10×25 time-frequency points (for 10 TRs), three for the 'sender' brain and three for the 'receiver' brain. Last and in order to simplify the analysis and to enhance the effect to noise ratio, the 25 frequency points were summed into 2 frequency bands: 'Low' corresponded to 0.013–0.04 Hz and 'high' corresponded to 0.04–0.1 Hz. Pathway indexes (Equation (4)) were calculated for each of these time-frequency points.

2.8. Networks selection- probabilistic approach

Two steps were used in the analysis, one to infer directionality, and two to test our hypotheses using a probabilistic approach. Our probabilistic approach was to count the number of times each region engaged in a process while keeping the changes for engagement equal. For these calculations, we categorized the regions into (1) regions in the 'sender' brain during the times it sends information; (2) regions in the 'sender' brain during the time it receives information; (3) regions in the 'receiver' brain during the time it receives information and (4) regions in the 'receiver' brain during the time it sends information. For the "4-regional networks", we had to define where to locate the four regions. Three possibilities exist. One is where all four regions are within one brain (sender or receiver), second when two regions in each brain and third when one region in one brain and three in the other. Since pathways in the first option could present non-JA interaction, this option was rejected. The second and third options guaranteed pathways of true JA interaction and therefore were used; the second option for the first analysis (i.e., using TPJ and dmPFC in each brain to infer directionality) and the third option for the probabilistic approach using the seven regions. Based on the original study that demonstrated the involvement of the TPJ and dmPFC in JA interaction (Bilek et al., 2015), we selected for the probabilistic approach either the TPJ or the dmPFC in one brain and three other regions (out of the other five) in the other brain. Fig. 1 illustrates these regional selections. Fig. 1A illustrates the case where three regions were in the sender brain and one either the dmPFC (top) or the TPJ (bottom) in the receiver brain, and Fig. 1B the case in which one region was in the sender brain and three in the receiver brain.

2.9. Statistical analysis

To define significant pathways, permutation nonparametric tests were used and the $PWI^k(\omega,t)'s$(Equation (4)) null distributions were calculated for each of the 9time points and the 2 frequency bands. Only nine time-points were used since few trials were shorter and of nine points only. The null distributions were calculated separately for the right and the left hemispheres, low and high frequencies, and the nine-time points. These distributions were calculated as follows: networks were constructed with 4 BOLD signals corresponding to the dmPFC and TPJ regions of one subject and the BOLD signals of the same regions from another subject. Random number generator was used to select the subjects from which the time-series were taken, keeping that the two selected subjects were not a real dyad. These regions were chosen for the following reasons: One is that the number of times the dmPFC and the TPJ were included in the calculated networks was higher than the number of times the other five regions were included. Second is the critical importance of these regions in inter-subject interaction, and third is our observation that the choice of regions had a minor effect on the null distributions (see below). For each network, $PWI^k(\omega,t)$(for a group of 27 pairs) were calculated 10000 times. Consequently, 10000 numbers were obtained (for each pathway, each time-frequency point and for the left and right hemispheres separately). These numbers were used to construct the null distributions and to calculate $PWI^k(\omega,t)$ of Equation (4) as a

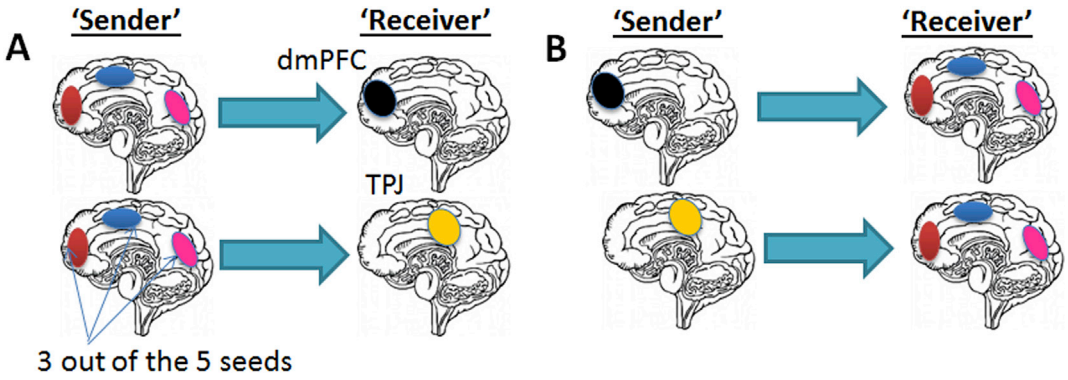

Fig. 1. Illustration of how regions were selected in the "4-regional networks". Networks were constructed with one region in one brain and three regions in the other brain. The single region was either the TPJ or the dmPFC and the three other regions were three out of the five other regions (the vmPFC, the PCC, the STS, the FFA, and the PreCue). (**A, top**) Networks with three regions in the 'sender' brain and the dmPFC in the 'receiver' brain. (**A, bottom**) Networks with three regions in the 'sender' brain and the TPJ in the 'receiver' brain. (**B, top**) Networks with three regions in the 'receiver' brain and the dmPFC in the 'sender' brain. **(B, bottom**) Networks with three regions in the 'receiver' brain and the TPJ in the 'sender' brain.

function of *cut*. $PWI^k(\omega,t,cut)$ were approximately invariant to time and pathway but differ for low and high frequencies and hemispheres. Cut_low_R = 0.15, Cut_high_R = 0.12, Cut_low_L = 0.13, Cut_high_L = 0.12 for low and high frequencies and for Right (R) and Left (L) hemispheres, all corresponded to $p < 0.002$, were chosen for all calculations. In order to test whether these cuts were specific to the above regions or general enough for all "4-regional networks", we calculated the null distributions for another regional choice. Specifically, we used the dmPFC in one brain and the vmPFC, PCC and the STS in the other. We obtained that the above *cut* values corresponded to $p < 0.0003$ for the low frequency and to $p < 0.01$ for the high-frequency bands, thus suggesting significant pathways for pathways with other regions for these cut values. To estimate confidence intervals (CI) and/or standard errors (SE), we used the bootstrap method with 1000 random resampling of the 27 dyads. CIs and SEs were calculated for each time -frequency point, each pathway, each frequency band and for the left and right hemispheres. To estimate CIs for the regional occurrences of specific processes (see below), we had to combine CIs of multiple time points. Due to the complexity of the "4-regional network" calculations (its multivariate nature and the multiple conditions needed), combining CIs (by either the MOVER (Zou and Donner, 2008) or the Propagating Imprecision approaches (Newcombe, 2011)) did not result with reasonable CIs. For that reason, we could only estimate the combined SE using the squaring and adding process (Newcombe, 2011). These SEs (values ± SE) were presented for all calculations. We note however that due to the complexity of the analysis, these SEs should be considered with caution.

Fig. 2 illustrates the different stages of the analysis.

3. Results

Fig. 3 shows the results for the "4-regional network" when the dmPFC and the TPJ were used in the 'sender' and the 'receiver' brains, for the case where these regions were in the right hemisphere. It gives the pathway index for significant pathways as a function of time along and after JA interaction ('Interaction' in the figure) with their bootstrap SEs. The analysis was performed with R1 = $dmPFC_s$; R2 = TPJ_s; R3 = $dmPFC_r$ and R4 = TPJ_r where R1 … R4 refer to the network's regions as given in Table 1 and the 's' and 'r' suffixes denote 'sender' and 'receiver' brains. Two pathways were significant, one for low frequency (shown in red) and the other for high frequency (shown in blue). The pathway at low frequency was significant for most of the time points while the one at high frequency was significant for the first time point (recalling that cutoff for low frequency was 0.15 and for high frequency, it was 0.12, see method). The former present continues interaction between the brains, while the latter interaction only during the 'interaction' period. We assume that the former is due to the face-to-face continues watching while the latter to information transferred between the brains due to the JA interaction. This last pathway corresponded to: $dmPFC_s$–TPJ_s– TPJ_r–$dmPFC_r$ (pathway # 5 in Table 1). To infer directed functional pathways, we have to assume the direction of flow i.e., if the signal is progressing from right to left or from left to right in the pathways of Table 1. Recall that the pathways in Table 1 are different in their temporal ranking but do not include directionality. To define directionality, we assume the obvious assumption, namely: the initial process between the brains in JA interaction is information flow from the 'sender' to the 'receiver'. This implies that directionality is from left to right in the pathways of Table 1. Using this assumption enables to change the pathways of Table 1 from hierarchical orders to directed pathways. It means that pathway # 5 is: $dmPFC_s \rightarrow TPJ_s \rightarrow TPJ_r \rightarrow dmPFC_r$. Similar to other directed coherence analyses, once directionality was defined in one network, it implies to all other networks. Consequently, the other significant pathway (i.e. s pathway # 10) reads $dmPFCr \rightarrow TPJ_r \rightarrow TPJ_s \rightarrow dmPFC_s$. The directed pathways for this "4-regional network" were a feedforward at high frequency and feedback at low frequency In both pathways, the two brains interacted through their TPJ regions. Fig. 3B illustrates these directed pathways with the dmPFC shown by a blue cluster and the TPJ by a red cluster. Colors of arrows presenting the directed pathways corresponded to the colors in Fig. 3A. In order to verify that these findings were not related to head motion, the sums and the differences of the mean frame-displacements of all dyads were correlated with the PWI values of these pathways for all time points and reference phases. The average Pearson correlation values over time points and reference phases were 0.065 ± 0.05 for the displacement difference and -0.08 ± 0.1 for displacement sum. These demonstrated that head motion didn't affect the results.

Table 2 lists all significant pathways that were obtained by calculating quadruplet networks with either the TPJ or the dmPFC in one brain and three other regions (out of the 5 remaining regions) in the other brain (as illustrated in Fig. 1) for the regions in the right (Table 2A) and in the left (Table 2B) hemispheres. To simplify the presentation, time points were grouped in three time-zones: time zone I (time points 1–3), time zone II (time points 4–6) and time zone III (time points 7–9). Pathways categorized by their time zones and frequency bands were included in these tables when their $PWI^k(\omega,t)$in at least one time point was significant. For easier visualization, the Tables were divided into pathways that included the dmPFC and to pathways that included the TPJ. As seen from these Tables, most of the significant pathways were at high frequency (32 versus 3 in the right hemisphere and 28 versus 10 in the left hemisphere), and there were more pathways that included the dmPFC versus pathways that included the TPJ (20 versus 12 in the right hemisphere and 19 versus 9 in the left hemisphere). To enable a qualitative study of the different processes and the regional involvements, we listed in Table 3 the number

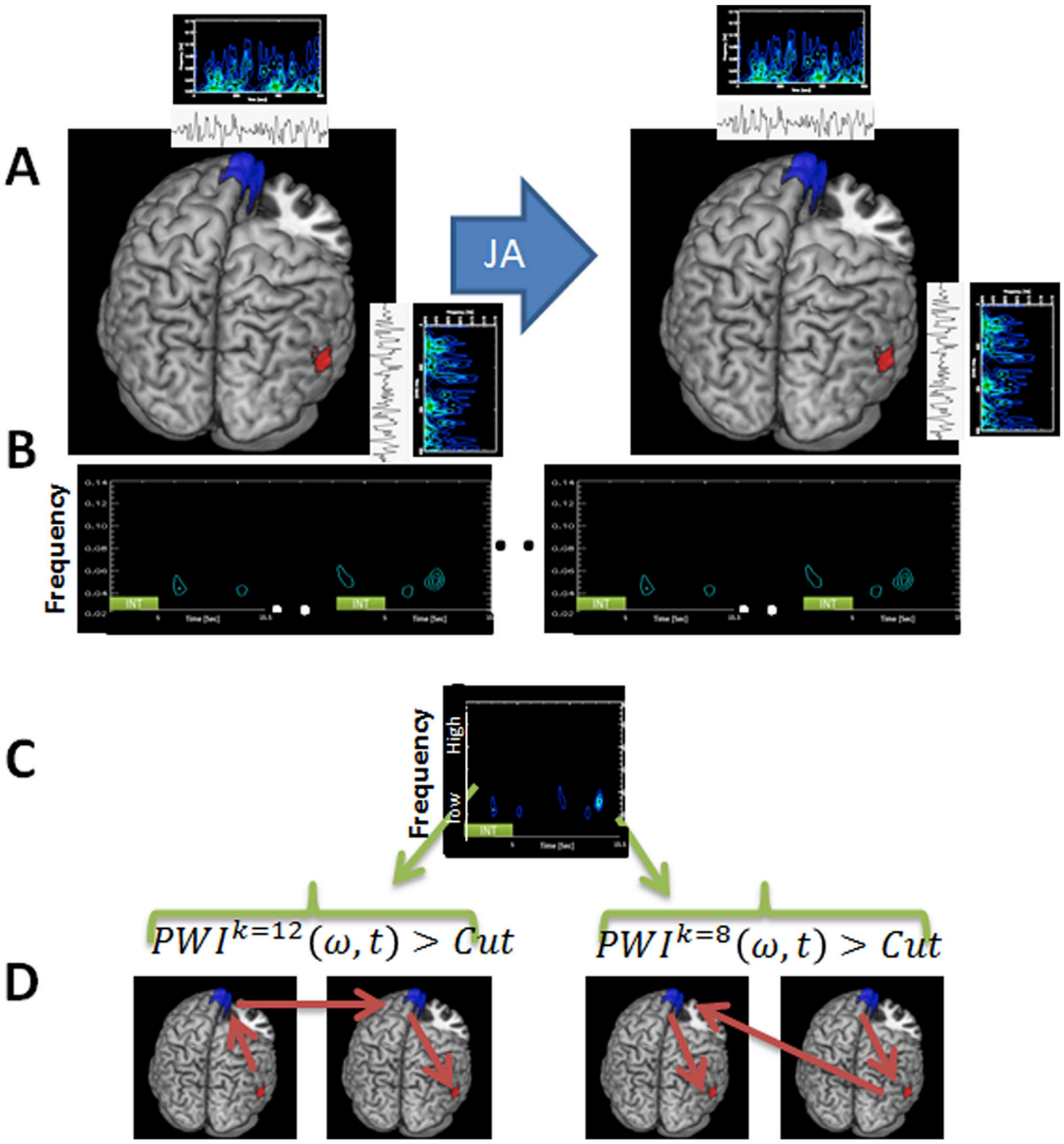

Fig. 2. Illustration of the multivariate directed functional connectivity analysis. For simplicity, illustration is shown for the case where the brain on the right was the sender and only for the sending process. **(A).** Four time-series from four regions in the two brains, each of 416 time-points (40 trials, each trial of 10 TRs) were extracted from the data and were wavelet transformed. In the illustration, the four time-series were the BOLD signals of the TPJ and dmPFC of the right hemisphere in both brains. **(B).** Equation (1) was used to obtain the three non-linear complex coherences (the amplitudes of two are shown). **(C).** All JA trials were summed together giving the time-frequency points of the brain when it was 'sending' information, and the time-frequency points of the brain when it was 'receiving' information. Additionally, the 25 frequency points were summed into 'Low' and 'high' frequencies (the 'sending' brain is shown). **(D).** Using Equation (4), directed pathways at each time-frequency point were calculated. Two significant pathways, each at a different time-frequency point, are shown.

of times each of the regions (vmPFC, PCC, STS, PreCue, and the FFA) appeared in the pathways of Table 2. These regions were categorized according to (I) the time zone (significant $PWI^k(\omega,t)$in time zone T1, T2 or T3), (II) whether the pathways included the dmPFC or the TPJ, and (III) the frequency (low or high). Regions in the Tables were divided to the following four processes: (1) Flow from the 'sender' to the 'receiver' and the regions were in the 'sender' brain (indicated in the table as S→R (S) and corresponding to initiating JA - IJA). (2) Flow from the 'receiver' to the 'sender' and the regions were in the 'sender' brain (R→S (S)). (3) Flow from the 'sender' to the 'receiver' and the regions were in the 'receiver' brain (S→R (R) and corresponding to responding JA - RJA), and (4) flow from the 'receiver' to the 'sender' and the regions were in the 'receiver' brain (R→S (R)). We note that while previous studies have tested the regional involvement during the IJA and the RJA processes(for example see (Redcay et al., 2012)), we are not aware of studies that studied the feedback processes. To clarify how we calculated the numbers in Table 3, consider for example the pathway STS→vmPFC→dmPFC→preCu with the dmPFC in the 'receiving' brain and the other three regions in the 'sender' brain. Assuming further that $PWI^k(\omega,t)$from Equation (4) was significant in time point 2 for the

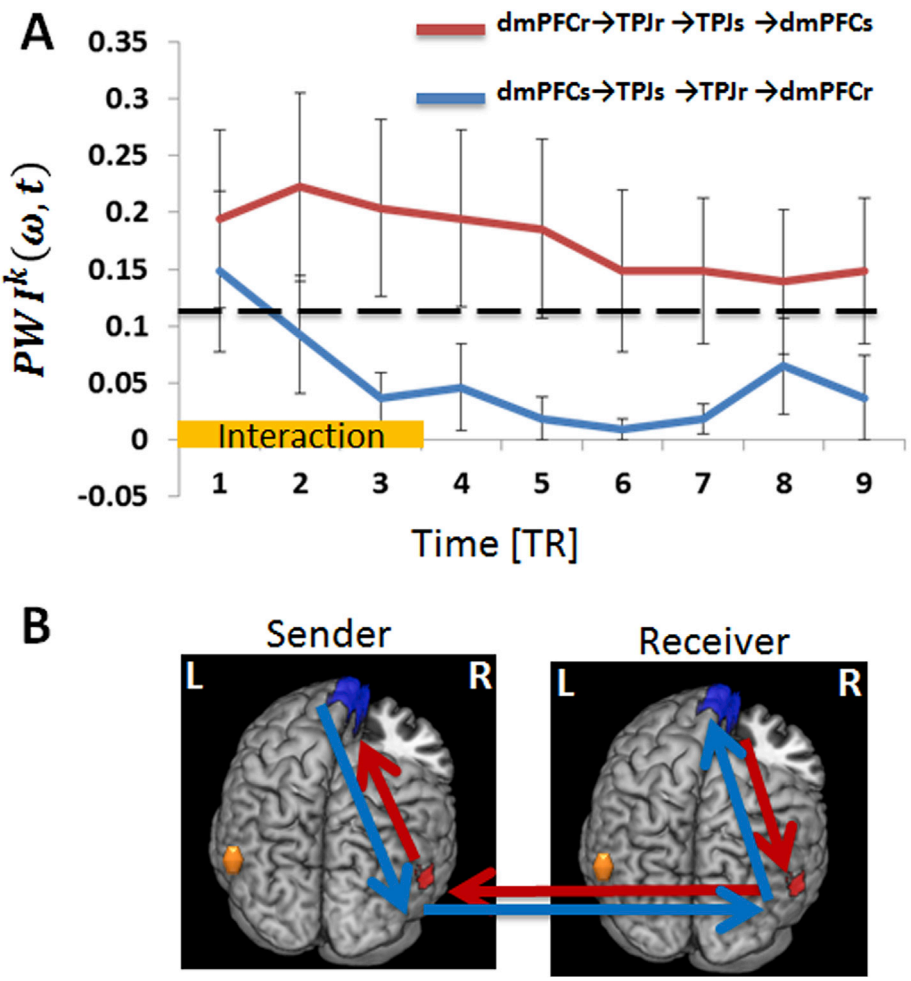

Fig. 3. (A). Pathway indexes ($PWI^k(\omega, t)$) as a function of time (TR = 1.55sec) during and after JA interaction ('Interaction' in the figure) for a network that included the $dmPFC_s$, TPJ_s, $dmPFC_r$ and TPJ_r of the right hemisphere with 's' and 'r' suffix denote 'sender' and 'receiver' brains. Significant pathways were defined when their $PWI^k(\omega, t)$in at least one time-point was above the cutoffs. $PWI^k(\omega,t)$are shown with their ± bootstrap standard errors. Two pathways were significant. One at high frequency (shown in blue and correspond to pathway # 5 in Table 1), and the other in low frequency (shown in red and corresponded to pathway # 10). Cutoffs were obtained from the corresponding null distributions and were for $p < 0.002$. For the high frequency, cutoff was 0.12 (shown by the dashed black line) and for the low frequency, it was 0.15. The time-invariant pathway at low frequency (shown in red) assumed to present continues interaction due to the mutual face watching. The time-dependent pathway (shown in blue), is expected to present JA interaction. Assuming that the initial JA process is information transfer from the 'sender' to the 'receiver' defines the directionality of all pathways in Table 1. Using this assumption, we list the directed pathways in the figure. In blue we show a feedforward pathway and in red a feedback pathway. **(B)** Illustration of these directed pathways with the dmPFC shown by blue clusters and the TPJ by red clusters. Pathway's color corresponded to the colors in A.

high-frequency range. For this case, the STS and the vmPFC were categorized to the S→R (S) process, while the precuneus to the R→S (S) process. For both cases, these regions were counted for high frequency and time zone I. Similar calculations were performed for all pathways in Table 2.

Fig. 4 gives the regional occurrences ± their bootstrap standard errors categorized by processes (S→R (S), R→S (S), S→R (R) and R→S (R), from Table 3) for pathways at high frequency that included the dmPFC or the TPJ. Fig. 4A for the right hemisphere, and Fig. 4B for the left hemisphere. This categorization enabled distinguishing between four processes: (1) A feedforward process; sender to receiver in the 'sending' and in the 'receiving' brains i.e., the IJA and the RJA processes. (2) A feedback process; flow from the 'receiver' to the 'sender' in the 'sending' and in the 'receiving' brains. (3) A sending process; a feedforward process in the 'sending' brain, and a feedback process in the 'receiver' brain. (4) A receiving process; a feedforward in the 'receiver' brain, and a feedback process in the 'sending' brain. For the right hemisphere (Fig. 4A), there were higher regional occurrences for the feedforward process (both IJA and RJA) versus the feedback processes for pathways with the dmPFC. Furthermore, higher regional occurrences where involved in the IJA process for pathways that included the TPJ. In addition, there were higher regional occurrences of the RJA process for pathways that included the dmPFC versus pathways that included the TPJ. For the left hemisphere (Fig. 4B), there were higher regional occurrences for the receiving process versus the sending process for pathways that included the TPJ. In addition, there were higher regional occurrences for the sending process for pathways that included the dmPFC versus pathways with the TPJ.

Fig. 5 gives the regional occurrences ± their bootstrap standard errors as a function of regions for pathways with the TPJ and pathways with the dmPFC for the right hemisphere (Fig. 5A) and the left hemisphere (Fig. 5B), using the same categorization as in Fig. 4. For the right hemisphere, pathways that included the TPJ, the vmPFC, the PCC and the STS were significantly more involved in the IJA process compared with other regions or other processes. Additionally, for the right hemisphere, pathways that included the dmPFC, the vmPFC, and the STS were significantly more involved in the IJA and the RJA processes compared with other regions and other processes. For the feedback processes, the FFA was more involved in receiving feedback in pathways with the TPJ of the right and the left hemispheres. Due to low occurrence values and high SE, inferring regional involvements for other processes was not possible.

4. Discussion

Understanding how our brain interacts during social contact is essential for the understanding of social interactions and can guide treatments in disorders characterized by social impairments. In this study, we identified cross-brain directed pathways that involve bidirectional information flow between brain systems of interacting subjects. We extended our novel directed functional connectivity analysis to track information-flow as functions of time and frequency of BOLD fMRI hyperscanning data. For social interaction, we choose to examine the simple JA paradigm in order to test our hypothesis that social contacts are bidirectional in nature. Furthermore, it enables testing whether initiation of JA and responding to JA use similar neural systems, whether JA initiates a feedback process, and whether sending and receiving processes are of

Table 2
Significant quadruplet directed pathways with either the TPJ or the dmPFC in one brain and three signals (out of the 5) in the other brain. Pathways are categorized by time zones, whether they include the TPJ or the dmPFC and in each brain and by frequency bands.

A. Right Hemisphere

dmPFC in the 'Receiver' brain

Low	High
Time Zone 1	
FFA ← dmpFC ← vmPFC ← STS	
STS ← Precu ← vmPFC ← dmpFC	
Time Zone 2	
FFA ← STS ← dmpFC ← vmPFC	
Time Zone 3	
vmPFC ← PCC ← dmpFC ← STS	
dmpFC ← PCC ← PreCu ← vmPFC	
PreCu ← dmpFC ← vmPFC ← PCC	
PreCu ← dmpFC ← vmPFC ← FFA	
dmpFC ← PreCu ← PCC ← STS	
dmpFC ← STS ← FFA ← PreCu	
PCC ← dmpFC ← PreCu ← FFA	

dmPFC in the 'Sender' brain

Low	High
Time Zone 1	
	vmPFC ← PCC ← STS ← dmpFC
	FFA ← PCC ← vmPFC ← dmpFC
	vmPFC ← STS ← dmpFC ← FFA
	vmPFC ← Precu ← dmpFC ← STS
	vmPFC ← Precu ← dmpFC ← FFA
	FFA ← Precu ← STS ← dmpFC
Time Zone 2	
	FFA ← PCC ← vmPFC ← dmpFC
	dmpFC ← vmPFC ← PCC ← FFA
Time Zone 3	
	FFA ← PreCu ← STS ← dmpFC
	FFA ← STS ← PreCu ← dmpFC

TPJ in the 'Receiver' brain

Low	High
Time Zone 1	
TPJ ← STS ← PCC ← vmPFC	
TPJ ← PreCu ← PCC ← vmPFC	
FFA ← STS ← PCC ← TPJ	
TPJ ← PreCu ← PCC ← STS	
PreCu ← TPJ ← STS ← PCC	
PreCu ← FFA ← STS ← TPJ	
Time Zone 2	
FFA ← TPJ ← vmPFC ← STS	
Time Zone 3	
TPJ ← STS ← vmPFC ← PCC	

TPJ in the 'Sender' brain

Low	High
Time Zone 1	
FFA ← PCC ← PreCu ← TPJ	PreCu ← PCC ← STS ← TPJ
Time Zone 2	
FFA ← PCC ← PreCu ← TPJ	
Time Zone 3	
FFA ← PCC ← PreCu ← TPJ	TPJ ← PCC ← PreCu ← vmPFC
	TPJ ← PreCu ← vmPFC ← PCC

B. Left Hemisphere

dmPFC in the 'Receiver' brain

Low	High
Time Zone 1	
dmPFC ← vmPFC ← PCC ← FFA	
FFA ← dmPFC ← vmPFC ← STS	
pre ← dmPFC ← vmPFC ← STS	
dmPFC ← STS ← PCC ← FFA	
Time Zone 2	
dmPFC ← vmPFC ← PCC ← FFA	
vmPFC ← PCC ← dmPFC ← pre	
STS ← pre ← PCC ← dmPFC	
dmPFC ← FFA ← PCC ← pre	
Time Zone 3	
STS ← vmPFC ← PCC ← dmPFC	
PCC ← vmPFC ← pre ← dmPFC	
pre ← PCC ← FFA ← dmPFC	

dmPFC in the 'Sender' brain

Low	High
Time Zone 1	
	FFA ← vmPFC ← STS ← dmPFC
	dmPFC ← STS ← vmPFC ← pre
	dmPFC ← PCC ← pre ← STS
Time Zone 2	
dmPFC ← FFA ← PCC ← pre	PCC ← dmPFC ← STS ← vmPFC
	STS ← dmPFC ← pre ← PCC
Time Zone 3	
vmPFC ← pre ← PCC ← dmPFC	vmPFC ← PCC ← pre ← dmPFC
dmPFC ← FFA ← PCC ← pre	FFA ← vmPFC ← STS ← dmPFC
	STS ← PCC ← pre ← dmPFC

TPJ in the 'Receiver' brain

Low	High
Time Zone 1	
FFA ← vmPFC ← PCC ← TPJ	
TPJ ← pre ← vmPFC ← PCC	
PCC ← FFA ← STS ← TPJ	
pre ← TPJ ← STS ← FFA	
Time Zone 2	
FFA ← vmPFC ← PCC ← TPJ	
Time Zone 3	

TPJ in the 'Sender' brain

Low	High
Time Zone 1	
STS ← TPJ ← PCC ← vmPFC	vmPFC ← FFA ← pre ← TPJ
TPJ ← vmPFC ← STS ← FFA	PCC ← pre ← TPJ ← STS
TPJ ← FFA ← STS ← PCC	
Time Zone 2	
STS ← FFA ← TPJ ← vmPFC	PCC ← pre ← TPJ ← STS
TPJ ← vmPFC ← STS ← FFA	
Time Zone 3	
TPJ ← vmPFC ← STS ← FFA	FFA ← PCC ← STS ← TPJ
TPJ ← FFA ← STS ← PCC	

similar regional mechanisms. In here, we focus on the TPJ and the dmPFC since previous findings demonstrated their critical involvement in social interaction (Redcay et al., 2012; Li et al., 2014; Mundy, 2018) regardless of the specific demand of a social task or social encounter (Schurz et al., 2014; Molenberghs et al., 2016).

The following assumptions were used in the analysis: (1) The time lag of the BOLD signals faithfully reproduces temporal precedence at the neuronal level. (2) Low and high frequencies of the BOLD signals corresponded to distinct neural frequencies and/or to different mechanisms. (3) The hemodynamic response functions were approximately equal across regions and subjects. (4) The analysis enables measuring dynamic processes and (5) the analysis can infer regional involvement. The first assumption is based on our (Goelman, Dan et al. 2017a,b, 2018) and other results. For example, previous fMRI studies (Mitra, Snyder et al. 2014, 2015a,b, 2015, 2016; Mitra et al., 2015; Mitra et al., 2017) showed that time-lag propagates within conventionally known resting-state networks and therefore can be used to infer fMRI signal progression and its directionality. In contrast, using computer simulations Smith et al. concluded that directionality is poorly predicted by time lags (Smith et al., 2011). In their study, they tested pairwise connectivity using Granger causality, condition independence, and Patel's pairwise conditional probability approaches. Pairwise connectivity using these methods

Table 3
Regional occurrences of pathway of Table 2. The number of times each region appeared in the pathways of Table 2 as function of time zone (T1, T2 or T3), frequency (low and high) and whether pathways included the dmPFC or the TPJ is listed. Further, pathways are divided to: flow from the 'sender' to the 'receiver' and regions were in the 'sender' brain (S→R (S)), flow from 'receiver' to 'sender' and regions were in the 'sender' brain (R→ S (S)), flow from 'sender' to the 'receiver' and regions were in the 'receiver' brain (S→ R (R)) and flow from the 'receiver' to the 'sender' and regions were in the 'receiver' brain (R→ S (R)).

A. Right Hemisphere

TPJ Low

	vmPFC			PCC			STS			PreCu			FFA		
	T1	T2	T3	T1	T2	T3	T1	T2	T3	T1	T2	T3	T1	T2	T3
S→R (S)															
R→S (S)															
S→R (R)				1	1	1				1	1	1	1	1	1
R→S (R)															

TPJ high

	vmPFC			PCC			STS			PreCu			FFA		
	T1	T2	T3	T1	T2	T3	T1	T2	T3	T1	T2	T3	T1	T2	T3
S→R (S)	2	1	1	4		1	3	1	1	2					
R→S (S)				1			2			2			2	1	
S→R (R)				1		1	1		1	1					1
R→S (R)			2			2						2			

dmPFC Low

	vmPFC			PCC			STS			PreCu			FFA		
	T1	T2	T3	T1	T2	T3	T1	T2	T3	T1	T2	T3	T1	T2	T3
S→R (S)															
R→S (S)															
S→R (R)															
R→S (R)															

dmPFC high

	vmPFC			PCC			STS			PreCu			FFA		
	T1	T2	T3	T1	T2	T3	T1	T2	T3	T1	T2	T3	T1	T2	T3
S→R (S)	1	1	3			3	1		3			4			3
R→S (S)	1		1			2	1	1		1		2	1	1	
S→R (R)	5	1		2	1		3		2	3		2	2	1	2
R→S (R)		1		2	1		1						2	1	

B. Left Hemisphere

TPJ Low

	vmPFC			PCC			STS			PreCu			FFA		
	T1	T2	T3	T1	T2	T3	T1	T2	T3	T1	T2	T3	T1	T2	T3
S→R (S)															
R→S (S)															
S→R (R)							1	1						1	
R→S (R)	2	2	1	2	1	1	2	1	2				2	1	2

TPJ high

	vmPFC			PCC			STS			PreCu			FFA		
	T1	T2	T3	T1	T2	T3	T1	T2	T3	T1	T2	T3	T1	T2	T3
S→R (S)	1			1			1			1			1		
R→S (S)	1	1		2	1		1			1			2	1	
S→R (R)	1			1	1	1			1	2	1		1		1
R→S (R)							1	1							

dmPFC Low

	vmPFC			PCC			STS			PreCu			FFA		
	T1	T2	T3	T1	T2	T3	T1	T2	T3	T1	T2	T3	T1	T2	T3
S→R (S)															
R→S (S)						1			1			1			
S→R (R)			1			1						1			
R→S (R)					1	1					1	1		1	1

dmPFC high

	vmPFC			PCC			STS			PreCu			FFA		
	T1	T2	T3	T1	T2	T3	T1	T2	T3	T1	T2	T3	T1	T2	T3
S→R (S)	3	1		2	2		3				2		2	2	
R→S (S)		1	2		2	3		1	1	1	1	2	1		1
S→R (R)			2		1	2	1	1	2			2	1		1
R→S (R)	1	1		1	1		2	1			1		2		

is significantly different from our method. In our method, we used the products of four wavelet coefficients thus the fourth order statistics of functional connectivity. This sort of characterization enables us to break the symmetries inherent in linear systems analyses and takes us into the realm of nonlinear coupling. Consequently, we claim that the simulations results of Smith et al. are not applicable to our method. Furthermore, using computer simulations with the Kuramoto model we have demonstrated correct directionality for a large range of coupling strength (Goelman and Dan, 2017a). For the second assumption of BOLD signal frequencies, we note that several studies have shown that BOLD frequencies contain physiological and/or neuronal information and were found to correlate preferentially with specific LFP frequency bands. For example, simultaneous recording of BOLD and LFP signals during spontaneous activity in early visual cortices of anesthetized monkeys showed that alpha, beta, and gamma LFP bands were informative about the BOLD signal with gamma the most informative band (Magri et al., 2012). Other studies suggested that BOLD oscillations frequencies uncover novel brain organizational rules, linking anatomical structures and functional networks to characteristic BOLD oscillations at specific frequencies (Baria et al., 2011). The third assumption of similar hemodynamic response functions across regions and subjects was grounded on the similarity between subjects and on the inter-individual correlations between time

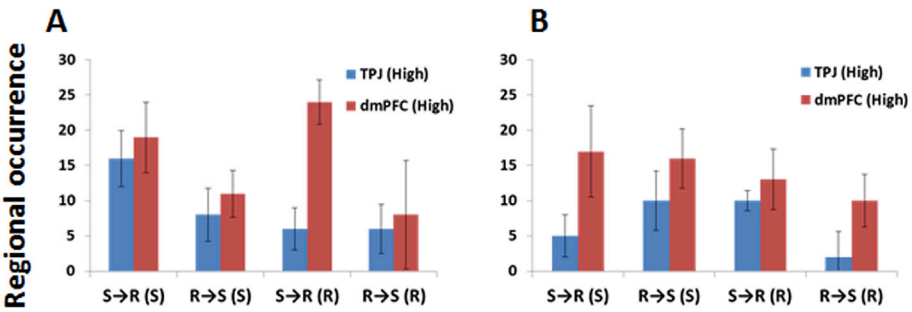

Fig. 4. Numbers of regions as a function of the four processes. Regional occurrences (from Table 3) are shown for pathways at high frequency for pathways that included either the dmPFC or the TPJ. Occurrence values are shown ± their bootstrap standard errors. S→R (S): Regional occurrences for flow from the 'sender' brain to the 'receiver' brain in the 'sender' brain. This corresponds to a feedforward process in the sender brain commonly named 'initiation of JA'. S→R (R): Regional occurrences for flow from the 'sender' brain to the 'receiver' brain in the 'receiver' brain. This corresponds to a feedforward process in the receiver brain commonly named 'responding to JA'. R→S (S): Regional occurrences for flow from the 'receiver' brain to the 'sender' brain in the 'sender' brain. This corresponds to a feedback process, i.e., receiving feedback. R→S (R): Regional occurrences for flow from the 'receiver' brain to the 'sender' brain in the 'receiver' brain. This corresponds to the initiation of a feedback process. **(A)** Results for the right hemisphere. **(B).** Results for the left hemisphere. dmPFC = dorsal medial prefrontal cortex, TPJ = temporoparietal junction.

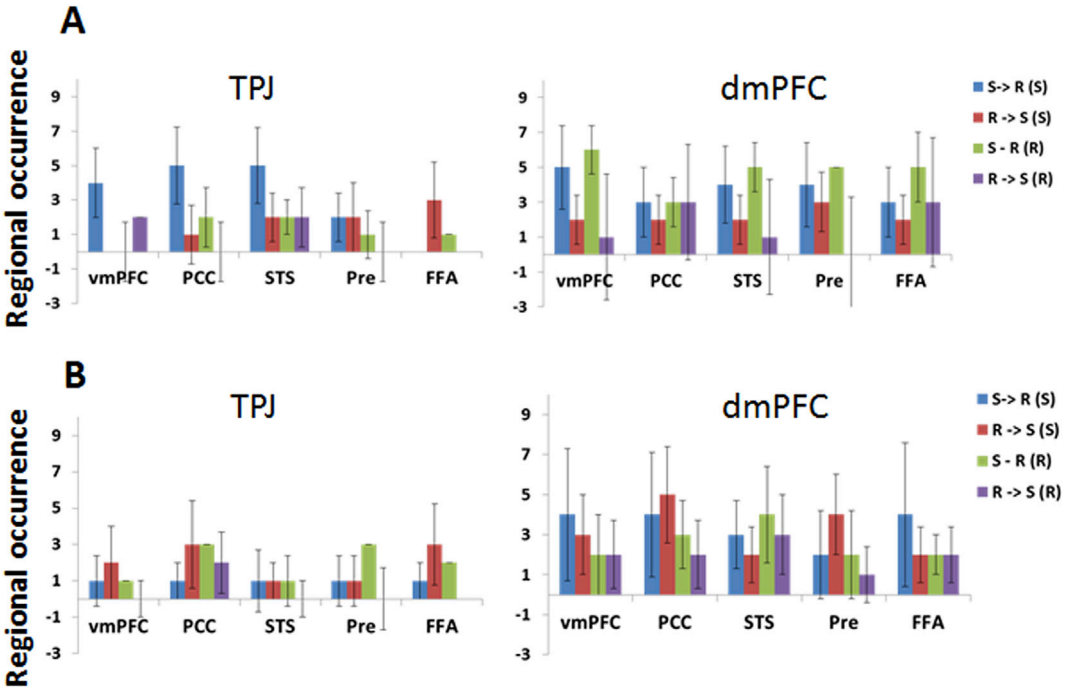

Fig. 5. Numbers of time regions were engaged in pathways, categorized by regions and processes for pathways at a high frequency that included either the dmPFC (right) or the TPJ (Left). Numbers of times are shown ± their bootstrap standard errors. S→R (S): Regional occurrences for flow from the 'sender' brain to the 'receiver' brain in the 'sender' brain. This corresponds to a feedforward process in the sender's brain commonly named 'initiation of JA'. S→R (R): Regional occurrences for flow from the 'sender' brain to the 'receiver' brain in the 'receiver' brain. This corresponds to a feedforward process in the receiver brain commonly named 'responding to JA'. R→S (S): Regional occurrences for flow from the 'receiver' brain to the 'sender' brain in the 'sender' brain. This corresponds to a feedback process, i.e., receiving feedback. R→S (R): Regional occurrences for flow from the 'receiver' brain to the 'sender' brain in the 'receiver' brain. This corresponds to the initiation of a feedback process. **(A)** Results for the right hemisphere. **(B).** Results for the left hemisphere. vmPFC = ventral medial prefrontal cortex, PCC = posterior cingulate cortex, STS = superior temporal sulcus, pre =precuneus, FFA = fusiform gyrus, dmPFC = dorsal medial prefrontal cortex, TPJ = temporoparietal junction.

courses. Specifically, all subjects were healthy right-handed females from the same city; of similar age and education; without a lifetime history of psychiatric or neurological illness or head trauma; and were not alcohol or drug abuse. Furthermore, in the original study (Bilek et al., 2015), cross-correlation (with a time lag) indicated that the rTPJ (and the mPFC) of the sender and the receiver brains were significantly coupled within a time window of 1–1.55sec (one TR). This suggests similar hemodynamic delay across all pairs. The fourth assumption, the ability to obtain dynamic information, is because the analysis is performed at each time-frequency point independently. Since local processing and recurrent connections could either increase or decrease phase differences, we limit ourselves to interpreting hierarchical ordering of phase delays of each time point in terms of unidirectional coupling. However, since the calculations in one-time point was independent on the calculations of other time points, different time points could have different directed pathways. For the assumption that the analysis can be used to obtain regional involvement, we note that the current limitation of the analysis, i.e., pathways of only four regions, prevented obtaining direct pathways of

many regions. Furthermore, the understanding that combining pathways is not allowed for a complex nonlinear system such as the brain, prevented obtaining long pathways of multiple regions. Instead, we used a probability strategy, i.e., counting the number of times regions were found within significant pathway while keeping the changes to be found equal. This enables to infer regional involvements for multiple regions ($n > 4$) of specific processes (e.g., feedforward or feedback) but, not to identify the exact multi-regional pathways of that processes. We further note that the choice of frequency bands, time zones, the regions used and anatomical rather than functional regions, probably affect the results. However, we assumed that these choices did not affect the main findings. Below we refer to the main findings and their possible neurophysiological meaning:

Feedforward, feedback, and hemispheres Most notable is our finding that JA interaction between two brains involving bidirectional information flow. To the best of our knowledge, this is the first study that demonstrated this intuitively expected behavior. We note that this finding has **important** consequences in the basic understanding of social interaction and in the treatment of social impairments. For example, it could suggest that social impairments can be differentiated to those that corresponds to the inability to understand social signals (impairment in social interaction) and those that have the inability to return signals (impairment in social communication). Table 3 and Fig. 4 show that the two hemispheres were differently involved in the feedforward and the feedback processes. The Table and Figure show higher regional occurrences of feedforward at high frequency: in the right hemisphere (65 regions versus 33 for feedback) and in the left hemisphere (45 versus 38). For low frequency, only one pathway was observed in the right hemisphere while regional occurrences in the left hemisphere were 6 for feedforward and 28 for feedback. These suggest that the right hemisphere was mostly engaged in the feedforward process (74 regions versus 33) and that the left hemisphere was more involved in the feedback process (51 feedforwards versus 66 feedbacks). Furthermore, pathways at low frequency and in the left hemisphere were mainly involved in a feedback process. *All together, these suggest a higher tendency for the right hemisphere to engage in a feedforward process, and a slightly high tendency of the left hemisphere to engage in a feedback process*.

TPJ versus dmPFC 66% of the regions in both hemispheres that were engaged in feedforward process (i.e. IJA + RJA) at high frequency were associated with the dmPFC while, only 34% were associated with the TPJ: 43 versus 22 in the right hemisphere and 30 versus 15 in the left hemisphere. Comparing regional occurrences of pathways that included the dmPFC or the TPJ between the four processes (Fig. 4) show the following: In the right hemisphere, the dmPFC engaged mainly with feedforward in both the IJA and the RJA processes, while no such difference was in the left hemisphere. The TPJ in the right hemisphere was mainly involved in the IJA process. In the left hemisphere, it was more engaged in the receiving processes (i.e. RJA and receiving feedback). Comparing regional occurrences between pathways of dmPFC and TPJ show that in the right hemisphere the dmPFC was more involved in the RJA process while in the left hemisphere it was more involved in sending processes (the IJA and feedback). For the feedback process, equal regional occurrences for initiating and receiving feedback process in the right hemisphere were observed for pathways with the TPJ and the dmPFC. In the left hemisphere, higher regional occurrences for initiation of the feedback process were observed for pathways with the dmPFC. *All the above suggest that the dmPFC is more involved in the sending process while the TPJ in the receiving process*.

These findings are in line with the intuitive understanding that receiving information is linked to the mirror system and with the knowledge that the TPJ is part of this system. The mirror system infers the state of others and was postulated to include visual input in the STS that is propagated to the TPJ and the inferior parietal lobes, and further to the premotor cortex (Van Overwalle, 2009). Furthermore, differences in TPJ and dmPFC functionality were reported before. For example, in a large meta-analysis study, temporary states such as goals, intentions, and desires of others were strongly engaged with the TPJ while inferring more enduring dispositions of others and the self, or interpersonal norms and scripts, engaged the medial prefrontal cortex (Van Overwalle, 2009). Whether these differences are related to feedforward and feedback processes as found by our study will have to be tested in the future.

Low and high frequencies Most pathways were significant at high frequency: 32 versus 1 in the right hemisphere and 25 versus 6 in the left hemisphere (Table 2). Inspections of these tables show a major difference between pathways at low and high frequencies. Whereas most pathways at high frequency were significant only in one time zone (all pathways in the right hemisphere and 22 out of 25 in the left hemisphere), most of the pathways at low frequency were significant at two or three time zones (1 out of 1 in the right hemisphere and 3 out of 6 in the left hemisphere). We suggest that the time-invariant pathways present a continuous interaction between the brains that is the result of the mutual face watching while time-dependent pathways corresponded to JA interaction. *It advises that two-brain interactions are encoded by the frequency: continues interaction by low fMRI frequencies and JA interaction by high fMRI frequencies*.

Regional involvement Fig. 5 gives the regional occurrences for the four different processes. It shows that in the right hemisphere the IJA and RJA processes were mainly involved with the dmPFC, the vmPFC, and the STS. Additionally, the IJA (but not the RJA) process was involved with the TPJ, vmPFC, PCC and the STS. *These suggest that the IJA and RJA have similar neural systems when the dmPFC is involved but a different one when the TPJ is involved*. Regarding the feedback process, high regional occurrences of the FFA in pathways with the TPJ at the right and left hemispheres suggest that these regions are part of the receiving feedback system. Several different virtual reality paradigms were used to study the common and distinct cognitive processes and neural systems involved in IJA and RJA in adults (Schilbach et al., 2010; Kim and Mundy, 2012; Redcay et al., 2012; Gordon et al., 2013; Caruana et al., 2015; Mundy, 2018) but none were conducted for the feedback process. Our results are partially in line with these studies with the limitation that our study tested only seven cortical regions.

Fig. 6 illustrates these main findings. Fig. 6A shows bidirectional flow with feedforward in the right hemisphere and feedback in the left hemisphere, with the dmPFC as the 'sender' and the TPJ as the 'receiver'. Fig. 6B illustrates the regional involvement of the feedforward process with equal involvements for IJA and RJA for pathways with the dmPFC and the regions involved in the IJA process for pathways with the TPJ.

To summarize, our study confirmed the hypothesis that JA interaction involved information flow in both directions between task partners. It further extended our understanding of the systems involved in these processes. We showed a high tendency of JA interaction for the feedforward process, and specifically of the right hemisphere and of pathways that included the dmPFC. The left hemisphere was shown to be more involved with feedback processes and particularly for pathways with the TPJ. We also suggest specific frequency dependency of these processes: JA interaction encoded by high fMRI frequencies versus continues interactions by lower fMRI frequencies. For the specific question that was studied by others namely are IJA and RJA uses the same or different neural systems, our results suggested the same systems for pathways with the dmPFC, but different systems for pathways with the TPJ. All these findings have important consequences in the basic understanding of social interaction and could aid in diagnosis and treatments of social impairments subjects. Further studies are needed to extend our understanding of the exact mechanism involved.

Author contribution

G.G.: Conception and design of the analysis, analysis and writing the paper.

R.D.: Data Preprocessing.

G.S.: Data Acquisition.

H.T, A.M. L.: Conception and design of the experimental study.

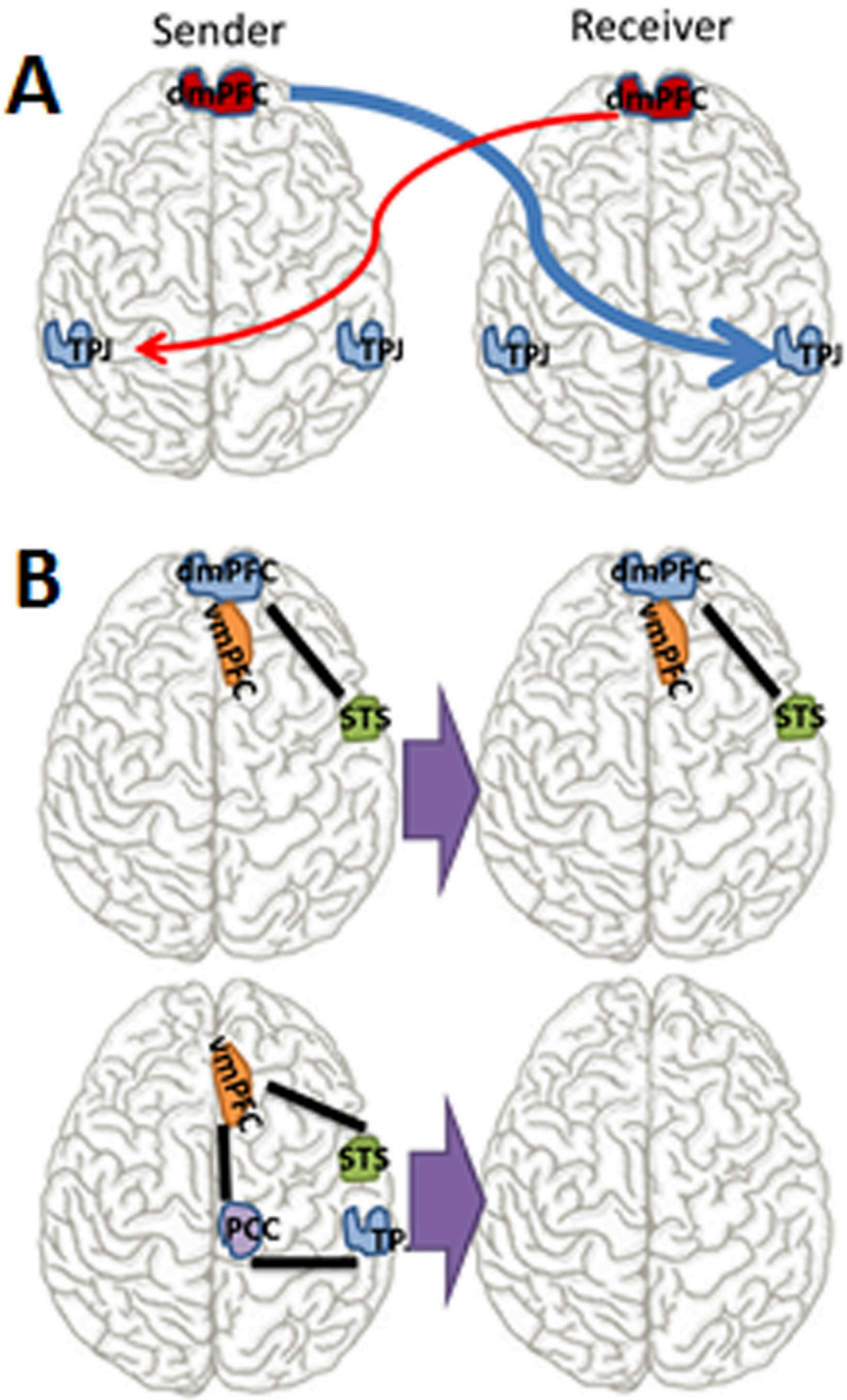

Fig. 6. Illustration of the main findings. **(A)**. Feedforward is mainly from the right hemisphere while feedback from the left hemisphere. Additionally, the sending process mainly engaged the dmPFC while the receiving process the TPJ. **(B)** Feedforward processes (the IJA and RJA) engaged the same regions for pathways with the dmPC but not of pathways with the TPJ.

E.B.: Data acquisition and participating in writing the paper.

Conflicts of interest

A.M.-L acknowledges support from the German Federal Ministry of Education and Research (BMBF, grants 01ZX1314G, 01GS08147, 01GQ1003B, 01GQ1102 subproject B7 and Collaborative Research Center 1158 subproject B09), European Union's Seventh Framework Programme (FP7, grants 602805, 602450, 115300 and HEALTH-F2-2010-241909), Innovative Medicines Initiative Joint Undertaking (IMI, grant 115008), Ministry of Science, Research and the Arts of the State of Baden-Wuerttemberg, Germany (MWK, grant 42-04HV.MED(16)/16/1). A.M.-L. has received consultant fees from American Association for the Advancement of Science, Atheneum Partners, Blueprint Partnership, Boehringer Ingelheim, Daimler und Benz Stiftung, Elsevier, F. Hoffmann-La Roche, ICARE Schizophrenia, K. G. Jebsen Foundation, L.E.K Consulting, Lundbeck International Foundation (LINF), R. Adamczak, Roche Pharma, Scioto Foundation, Sumitomo Dainippon Pharma, Seattle

Foundation – Alzheimer Research Switzerland, System Analytics, and has received lectures fees including travel fees from Boehringer Ingelheim, Fama Public Relations, Institut d'investigacions Biomèdiques August Pi i Sunyer (IDIBAPS), Janssen-Cilag, Klinikum Christophsbad, Göppingen, Lilly Deutschland, Luzerner Psychiatrie, LVR Klinikum Düsseldorf, LWL Psychiatrie Verbund Westfalen-Lippe, Otsuka Pharmaceuticals, Reunions i Ciencia S. L., Spanish Society of Psychiatry, Südwestrundfunk Fernsehen, Stern TV, and Vitos Klinikum Kurhessen. A.M.-L. and P.K. acknowledge support from to German Research Foundation (DFG, ME 1591/4-1). H.T. acknowledges support from the German Federal Ministry of Education and Research (BMBF, grant 01GQ1102) and the German Research Foundation (DFG, TO 539/3-1).

G.G acknowledges the support of the Anges Ginges found and the research authority of the Hadassah Medical Center.

Appendix A. Supplementary data

Supplementary data to this article can be found online at https://doi.org/10.1016/j.neuroimage.2019.05.028.

References

Babiloni, F., Astolfi, L., 2014. Social neuroscience and hyperscanning techniques: past, present and future. Neurosci. Biobehav. Rev. 44, 76–93.
Balconi, M., Vanutelli, M.E., 2017. Brains in competition: improved cognitive performance and inter-brain coupling by hyperscanning paradigm with functional near-infrared spectroscopy. Front. Behav. Neurosci. 11, 163.
Baria, A.T., Baliki, M.N., Parrish, T., Apkarian, A.V., 2011. Anatomical and functional assemblies of brain BOLD oscillations. J. Neurosci. 31 (21), 7910–7919.
Bianciardi, M., Fukunaga, M., van Gelderen, P., de Zwart, J.A., Duyn, J.H., 2011. Negative BOLD-fMRI signals in large cerebral veins. J. Cereb. Blood Flow Metab. 31 (2), 401–412.
Bilek, E., Ruf, M., Schafer, A., Akdeniz, C., Calhoun, V.D., Schmahl, C., Demanuele, C., Tost, H., Kirsch, P., Meyer-Lindenberg, A., 2015. Information flow between interacting human brains: identification, validation, and relationship to social expertise. Proc. Natl. Acad. Sci. U. S. A. 112 (16), 5207–5212.
Bilek, E., Stossel, G., Schafer, A., Clement, L., Ruf, M., Robnik, L., Neukel, C., Tost, H., Kirsch, P., Meyer-Lindenberg, A., 2017. State-dependent cross-brain information flow in borderline personality disorder. JAMA Psychiatry 74 (9), 949–957.
Bzdok, D., Langner, R., Schilbach, L., Jakobs, O., Roski, C., Caspers, S., Laird, A.R., Fox, P.T., Zilles, K., Eickhoff, S.B., 2013. Characterization of the temporo-parietal junction by combining data-driven parcellation, complementary connectivity analyses, and functional decoding. Neuroimage 81, 381–392.
Caruana, N., Brock, J., Woolgar, A., 2015. A frontotemporoparietal network common to initiating and responding to joint attention bids. Neuroimage 108, 34–46.
Chai, X.J., Castanon, A.N., Ongur, D., Whitfield-Gabrieli, S., 2011. Anticorrelations in resting state networks without global signal regression. Neuroimage 59 (2), 1420–1428.
Fox, M.D., Zhang, D., Snyder, A.Z., Raichle, M.E., 2009. The global signal and observed anticorrelated resting state brain networks. J. Neurophysiol. 101 (6), 3270–3283.
Goelman, G., Dan, R., 2017a. Multiple-region directed functional connectivity based on phase delays. Hum. Brain Mapp. 38 (3), 1374–1386.
Goelman, G., Dan, R., Keadan, T., 2018. Characterizing directed functional pathways in the visual system by multivariante nonlinear coherence of fMRI data. Sci. Rep. 5 (8).
Goelman, G., Dan, R., Ruzicka, F., Bezdicek, O., Ruzicka, E., Roth, J., Vymazal, J., Jech, R., 2017. Frequency-phase analysis of resting-state functional MRI. Sci. Rep. 7, 43743.
Goelman, G., Gordon, N., Bonne, O., 2014. Maximizing negative correlations in resting-state functional connectivity MRI by time-lag. PLoS One 9 (11), e111554.
Gordon, I., Eilbott, J.A., Feldman, R., Pelphrey, K.A., Vander Wyk, B.C., 2013. Social, reward, and attention brain networks are involved when online bids for joint attention are met with congruent versus incongruent responses. Soc. Neurosci. 8 (6), 544–554.
Hari, R., Henriksson, L., Malinen, S., Parkkonen, L., 2015. Centrality of social interaction in human brain function. Neuron 88 (1), 181–193.
Kim, K., Mundy, P., 2012. Joint attention, social-cognition, and recognition memory in adults. Front. Hum. Neurosci. 6, 172.
Koike, T., Tanabe, H.C., Okazaki, S., Nakagawa, E., Sasaki, A.T., Shimada, K., Sugawara, S.K., Takahashi, H.K., Yoshihara, K., Bosch-Bayard, J., Sadato, N., 2016. Neural substrates of shared attention as social memory: a hyperscanning functional magnetic resonance imaging study. Neuroimage 125, 401–412.
Li, W., Mai, X., Liu, C., 2014. The default mode network and social understanding of others: what do brain connectivity studies tell us. Front. Hum. Neurosci. 8, 74.
Liu, D., Liu, S., Liu, X., Zhang, C., Li, A., Jin, C., Chen, Y., Wang, H., Zhang, X., 2018. Interactive brain activity: review and progress on EEG-based hyperscanning in social interactions. Front. Psychol. 9, 1862.
Magri, C., Schridde, U., Murayama, Y., Panzeri, S., Logothetis, N.K., 2012. The amplitude and timing of the BOLD signal reflects the relationship between local field potential power at different frequencies. J. Neurosci. 32 (4), 1395–1407.
Mitra, A., Snyder, A.Z., Blazey, T., Raichle, M.E., 2015. Lag threads organize the brain's intrinsic activity. Proc. Natl. Acad. Sci. U. S. A. 112 (17), E2235–E2244.
Mitra, A., Snyder, A.Z., Constantino, J.N., Raichle, M.E., 2017 Feb 1. The lag structure of intrinsic activity is focally altered in high functioning adults with autism. Cerebr. Cortex 27 (2), 1083–1093. https://doi.org/10.1093/cercor/bhv294.
Mitra, A., Snyder, A.Z., Hacker, C.D., Pahwa, M., Tagliazucchi, E., Laufs, H., Leuthardt, E.C., Raichle, M.E., 2016. Human cortical-hippocampal dialogue in wake and slow-wave sleep. Proc. Natl. Acad. Sci. U. S. A. 113 (44), E6868–E6876.
Mitra, A., Snyder, A.Z., Hacker, C.D., Raichle, M.E., 2014. Lag structure in resting-state fMRI. J. Neurophysiol. 111 (11), 2374–2391.
Molenberghs, P., Johnson, H., Henry, J.D., Mattingley, J.B., 2016. Understanding the minds of others: a neuroimaging meta-analysis. Neurosci. Biobehav. Rev. 65, 276–291.
Mundy, P., 2018. A review of joint attention and social-cognitive brain systems in typical development and autism spectrum disorder. Eur. J. Neurosci. 47 (6), 497–514.
Murphy, K., Birn, R.M., Handwerker, D.A., Jones, T.B., Bandettini, P.A., 2009. The impact of global signal regression on resting state correlations: are anti-correlated networks introduced? Neuroimage 44 (3), 893–905.
Newcombe, R.G., 2011. Propagating imprecision: combining confidence intervals from independent sources. Commun. Stat. Theor. Methods 40 (3154–3180), 3154–3180.
Power, J.D., Mitra, A., Laumann, T.O., Snyder, A.Z., Schlaggar, B.L., Petersen, S.E., 2014. Methods to detect, characterize, and remove motion artifact in resting state fMRI. Neuroimage 84, 320–341.
Redcay, E., Kleiner, M., Saxe, R., 2012. Look at this: the neural correlates of initiating and responding to bids for joint attention. Front. Hum. Neurosci. 6, 169.
Schilbach, L., Timmermans, B., Reddy, V., Costall, A., Bente, G., Schlicht, T., Vogeley, K., 2013. Toward a second-person neuroscience. Behav. Brain Sci. 36 (4), 393–414.
Schilbach, L., Wilms, M., Eickhoff, S.B., Romanzetti, S., Tepest, R., Bente, G., Shah, N.J., Fink, G.R., Vogeley, K., 2010. Minds made for sharing: initiating joint attention recruits reward-related neurocircuitry. J. Cogn. Neurosci. 22 (12), 2702–2715.
Schippers, M.B., Roebroeck, A., Renken, R., Nanetti, L., Keysers, C., 2010. Mapping the information flow from one brain to another during gestural communication. Proc. Natl. Acad. Sci. U. S. A. 107 (20), 9388–9393.
Schurz, M., Radua, J., Aichhorn, M., Richlan, F., Perner, J., 2014. Fractionating theory of mind: a meta-analysis of functional brain imaging studies. Neurosci. Biobehav. Rev. 42, 9–34.
Smith, S.M., Miller, K.L., Salimi-Khorshidi, G., Webster, M., Beckmann, C.F., Nichols, T.E., Ramsey, J.D., Woolrich, M.W., 2011. Network modelling methods for FMRI. Neuroimage 54 (2), 875–891.
Stam, C.J., Nolte, G., Daffertshofer, A., 2007. Phase lag index: assessment of functional connectivity from multi channel EEG and MEG with diminished bias from common sources. Hum. Brain Mapp. 28 (11), 1178–1193.
Stam, C.J., van Straaten, E.C., 2012. Go with the flow: use of a directed phase lag index (dPLI) to characterize patterns of phase relations in a large-scale model of brain dynamics. Neuroimage 62 (3), 1415–1428.
Torrence, C., Compo, G.P., 1998. Wavelet analysis. Bull. Am. Meteorol. Soc. 79, 61–78.
Van Overwalle, F., 2009. Social cognition and the brain: a meta-analysis. Hum. Brain Mapp. 30 (3), 829–858.
Weissenbacher, A., Kasess, C., Gerstl, F., Lanzenberger, R., Moser, E., Windischberger, C., 2009. Correlations and anticorrelations in resting-state functional connectivity MRI: a quantitative comparison of preprocessing strategies. Neuroimage 47 (4), 1408–1416.
Whitfield-Gabrieli, S., Nieto-Castanon, A., 2012. Conn: a functional connectivity toolbox for correlated and anticorrelated brain networks. Brain Connect. 2 (3), 125–141.
Zou, G.Y., Donner, A., 2008. Construction of confidence limits about effect measures: a general approach. Stat. Med. 27 (10), 1693–1702.